Landslides and Engineered Slopes: Protecting Society through Improved Understanding – Eberhardt et al. (eds)
© 2012 Taylor & Francis Group, London, ISBN 978-0-415-62123-6

Terrestrial photogrammetry and LiDAR investigation of the cliffs associated with the seismically triggered rockfalls during the February and June 2011 Christchurch earthquakes

M.-A. Brideau
School of Environment, University of Auckland, Auckland, New Zealand

C.I. Massey & G. Archibald
GNS Science, Avalon, New Zealand

M. Jaboyedoff
Institut de Géomatique et d'Analyse du Risque, Université de Lausanne

ABSTRACT: The February 22 and June 13, 2011 Christchurch earthquakes (Mw 6.2 and 6.0 respectively), on the South Island of New Zealand, triggered widespread rockfall activity in the Port Hills area. Due to the epicentre locations, large amount of energy released, and the steep topography; Peak Ground Accelerations (PGA) of 2.2 g were recorded in the hills south east of Christchurch. The local bedrock geology consists of Miocene basaltic lava flows with interbeds of breccia and tuff. Terrestrial photogrammetry and laser scanning techniques were used to characterize the rock masses in cliffs at three fieldsites that experience rockfall activity. The advantages and limitations of each technique are discussed in terms of the discontinuity pattern mapped, and orientation biases.

1 INTRODUCTION

The Canterbury region on the east coast of the central South Island of New Zealand experienced 3 large earthquakes between September 2010 and June 2011. While the September 4, 2010 earthquake was the largest with a Mw of 7.1 (Gledhill et al. 2011) it triggered relatively few mass movements (Massey et al. 2010) as its epicentre was located in the low relief rural area near Darfield (Fig. 1). The surface deformation features associated with the September earthquake are summarized in Barrell et al. (2011) while the geotechnical aspects of the ground and infrastructure response are discussed in Allen et al. (2010) and Beetham (2011).

The epicentres of the February 22, 2011 (Mw 6.2) and June 13, 2011 (Mw 6.0) earthquakes were located in the hilly area of the Port Hills and closer to the large urban centre of Christchurch (Fig. 1). The epicentre location, along with the large amount of energy released, and the steep topography; led to recorded peak ground accelerations (PGA) of 2.2 g in the hills south east of Christchurch (Fry et al. 2011). This violent ground shaking resulted in widespread damage to infrastructure and the initiation of rockfalls and deep-seated landslides (Davey 2011, Hancox & Perrin 2011, Hancox et al. 2011, Massey & Dellow 2011, Reyners 2011).

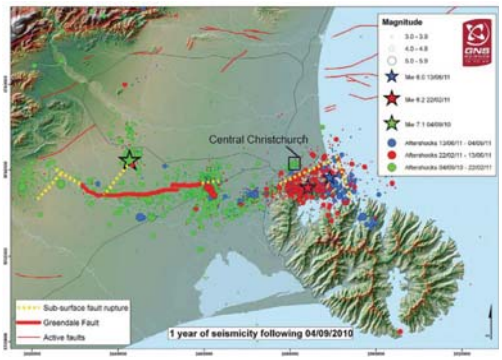

Figure 1. Location of the epicentres of the three large earthquakes that have affected the Canterbury region and the associated sequence of aftershocks (www.geonet.org.nz).

1.1 *Study area*

The Port Hills area consists of the 400–500 m high dissected flank of an extinct volcano (Sewell et al. 1992). The bedrock geology consists of Miocene basaltic lava flows with interbeds of breccia and tuff (Brown & Webber 1992). The majority of the rockfall activity occurred along abandoned sea

cliffs and quarries but a few road cuts and natural slopes were also affected. The cliffs associated with the abandoned quarries were typically between 20–70 m high and had slope angles between 70° and vertical. Minor rockfall activity had been previously recorded in the Port Hills area (Brown & Webber 1992).

Figure 2. Location map of the three sites discussed in this paper (Image from Google Earth).

Figure 3. Overview of the a) western and b) northern wall at the Redcliffs school fieldsite.

Figure 4. Overview of the Peacock's Gallop fieldsite. Note the paleochannel in the central upper part of the cliff and the use of shipping containers as rockfall barrier.

Figure 5. Overview of the geology and rockfall talus at the Wakefield Terrace fieldsite.

This paper will concentrate on three sites in the Port Hills area that are abandoned sea cliffs (Fig. 2). The first site is the Redcliffs School (Fig. 3), the second is Peacock's Gallop (Fig. 4), and the third is Wakefield Terrace (Fig. 5) in the locality of Sumner.

2 METHODOLOGY

2.1 *Terrestrial photogrammetry*

Terrestrial photogrammetry was the primary method used in this study to collect discontinuity orientation and characteristics data. Sturzenegger & Stead (2009a, b) have demonstrated its applicability to assess the orientation of discontinuities in large natural rock slopes and open pits. The digital imagery analysed in this project was acquired using a Nikon 300s digital

camera with 50 mm and 105 mm focal length lenses. The images obtained were processed using the software Siro3D and SiroJoint (CSIRO 2010). The position of the camera was determined in the field using a real time kinematic global positioning system (RTK GPS) which along with the bearing of the line of sight of the camera was used to geo-reference the 3D models created using the Siro3D software. The orientation and persistence was extracted from the 3D models by defining a plane or trace corresponding to a discontinuity in SiroJoint (Fig. 6). These software have previously been used successfully to collect orientation data in large road cuts in the United States (Haneberg 2008) and coal mines in Australia (Maconochie et al. 2010).

2.2 *COLTOP-3D*

The software COLTOP-3D (Jaboyedoff et al. 2004) was used to extract structural information from the terrestrial LiDAR dataset for each of the three field sites. COLTOP-3D derives ground surface orientation based on the x, y, z positional data from airborne or terrestrial LiDAR data. COLTOP-3D assigns a colour to each cell in the DEM based on the dip and dip direction orientation of its pole. In the resulting hillshade, extensive zones of constant orientation (Fig. 7) are highlighted and are assumed to represent a structural surface (bedding, persistent joints, faults). These zones of constant orientation are manually identified by the user. COLTOP-3D has been previously used successfully on several rock slope stability case studies to generate stereonets of structures (e.g. Jaboyedoff et al. 2009, Oppikofer et al. 2009, Pedrazzini et al. 2010, Brideau et al. 2011, Jaboyedoff et al. 2011, Oppikofer et al. 2011).

The terrestrial LiDAR data was collected using a Riegl Z420i laser scanner. The resulting point clouds were geo-referenced using static GPS techniques. Multiple point clouds were combined and processed in the software RiSCAN Pro from Riegl. The average point spacing of the processed data was 0.1 m. Laser scans were collected after the February and June 2011 earthquakes.

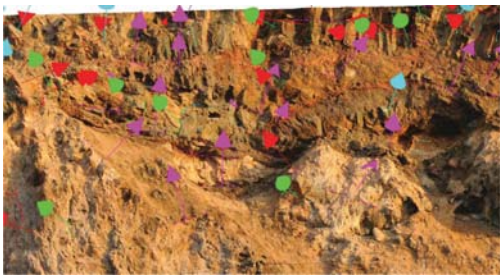

Figure 6. Example of the 3D model created based on the terrestrial photogrammetry for the Wakefield Terrace fieldsite.

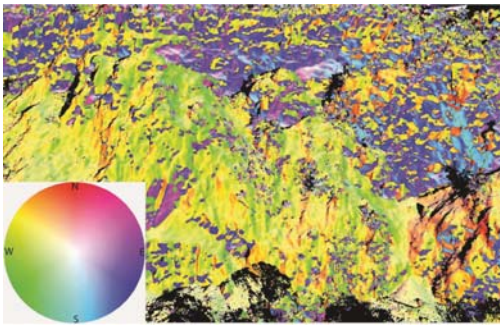

Figure 7. Example of the orientation hillshade created based on the terrestrial LiDAR data for the Wakefield Terrace fieldsite.

3 RESULTS

3.1 *Terrestrial photogrammetry*

A total of 16 digital photogrammetric pairs were collected on June 15–17, 2011. From these, 1402 discontinuities were identified in the 3D models. The overall fracturing pattern was found to be similar at all three sites (Table 1 and Fig. 8). Three to four steeply dipping discontinuity sets along with a sub-horizontal one were identified which is consistent with a columnar jointed rock mass. The minor differences in the mean orientation of the discontinuity sets is attributed to local variation in the paleotopography during the emplacement of the geologic units and orientation bias due to the outcrops orientation.

3.2 *Terrestrial LiDAR*

Due to ongoing aftershocks following the June 13, 2011 earthquake it was impossible to directly access the base of the cliff to collect discontinuity measurements for comparison with the terrestrial photogrammetry data. The laser scanning point clouds collected to document the evolution of the cliff face associated with the seismically triggered rock fall activity were analysed in COLTOP-3D. This provided an independent dataset to corroborate the results from the photogrammetry. A total of approximately 125 individual planar surfaces were identified in the laser scanning data for the three field sites. The stereonets in Figure 9 plot the poles to each DEM cell included when defining a planar surface. The summary of the

Table 1. Summary of the mean discontinuity set orientations identified using the terrestrial photogrammetry technique at each field site. DD = Dip Direction.

	Redcliffs	Peacock's	Wakefield
Discontinuity	Dip/DD	Dip/DD	Dip/DD
DS1	84°/190°	76°/198°	76°/233°
DS2	87°/091°	84°/240°	89°/097°
DS3	83°/126°	87°/157°	86°/156°
DS4	52°/067°	61°/025°	80°/034°
Bedding	19°/033°	24°/030°	17°/090°

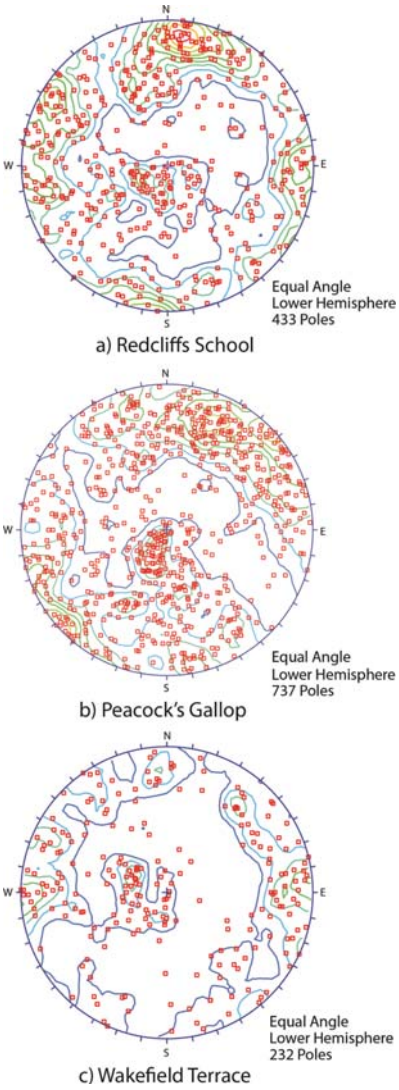

Figure 8. Stereographic projection of the poles to the discontinuities measured in the 3D models for a) Redcliffs School, b) Peacock's Gallop, and c) Wakefield Terrace.

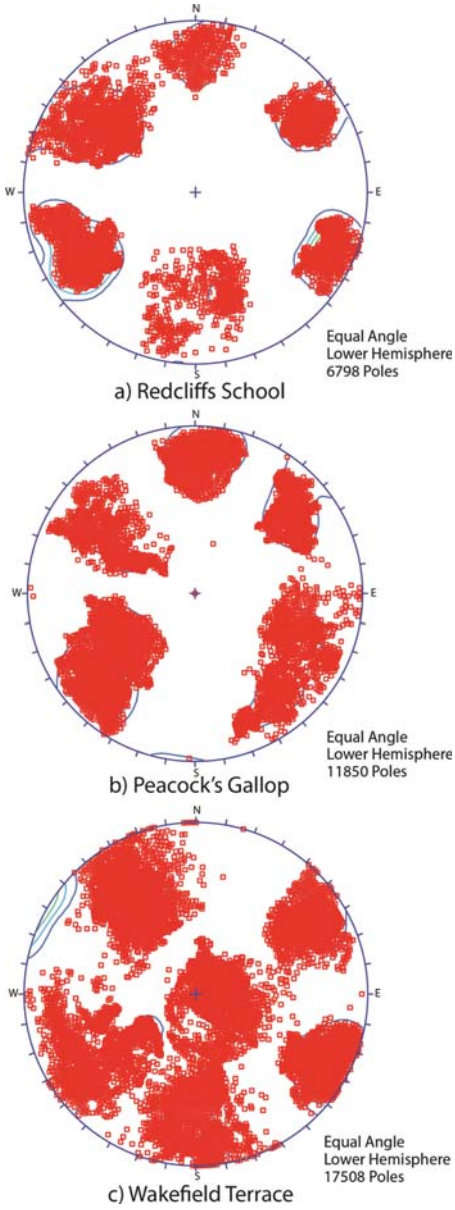

Figure 9. Stereographic projection of the poles to the planar surfaces measured using the terrestrial LiDAR dataset and the software COLTOP for a) Redcliffs School, b) Peacock's Gallop, and c) Wakefield Terrace.

surface orientation families which are assumed to represent discontinuities sets is presented in Table 2. Six steeply dipping surface orientation families were identified. As these discontinuity sets are steeply dipping, they get assigned a different colour if the pole plots on one side or the other

Table 2. Summary of the mean discontinuity set orientations identified using the terrestrial LiDAR dataset and the software COLTOP-3D at each field site. DD = Dip Direction.

	Redcliffs	Peacock's	Wakefield
Discontinuity	Dip/DD	Dip/DD	Dip/DD
DS1	77°/180°	77°/183°	NA
DS2	81°/294°	68°/289°	81°/298°
DS3	68°/125°	62°/122°	64°/147°
DS4	74°/062°	64°/052°	61°/060°
DS5	75°/236°	73°/231°	75°/238°
DS6	63°/355°	76°/323°	70°/359°
Bedding	NA	NA	13°/272°

of the great circle. This means for example that DS 4 and DS 5 in Table 2 could represent the same discontinuity set which straddles the great circle.

Since 7 surfaces were defined for each surface orientation family (discontinuity set) identified, this approach provides an approximation of the extent (persistence) of each of the discontinuity sets (i.e. the surfaces with the greater area are represented by a greater number of poles to the DEM cell).

4 DISCUSSION

While the discontinuity set patterns identified by the terrestrial photogrammetry and LiDAR datasets were similar, some differences were observed. The shallowly dipping discontinuities were noticeably absent from the LiDAR dataset for the Redcliffs School and Peacock's Gallop fieldsites. Sturzenegger and Stead (2009a) discussed that an occlusion orientation bias prevents lasers to be reflected from the surfaces that have an orientation similar to the line of sight of the laser scanner and they cannot be represented in COLTOP-3D as a coloured cell hillshade. The photographic camera had a line of sight similar to the laser scanner but the shallowly dipping discontinuities could be defined by fitting a plane to the trace in the rock outcrop. This is considered to reduce the importance of the occlusion bias. Using the datasets available in this study, the terrestrial photogrammetry method is considered to be more effective at delineating discontinuities that have a dip direction and dip similar to the line of sight of the laser scanner. The orientation bias in the terrestrial LiDAR dataset could be reduced by acquiring laser scans with varying line of sight angle and combined them.

There are two differences in the approach of identifying discontinuities between the techniques used in this study. In the photogrammetry all discontinuities in the 3D models were mapped while in COLTOP-3D only repeating surfaces with the same colour orientation were identified. These would be analogous to the area vs. subjective field mapping techniques. The scale of observation at which the measurements were made was also different between techniques. In the photogrammetry the discontinuities were identified at the decimetre to metre scale while the discontinuities in the LiDAR represented features at the metre to decametre scale.

Approximately 75% of the discontinuity planes or traces identified in the photogrammetry were from the columnar basalt geological unit. To assess the importance of this sampling bias Figure 10 compares the stereonets of the poles to the discontinuities obtained from the columnar basalt and breccia (including pyroclastics and tephra) units. There does not appear to be significant differences in the discontinuity pattern between the different geological units. The thinner depositional thicknesses of columnar basalt unit led to

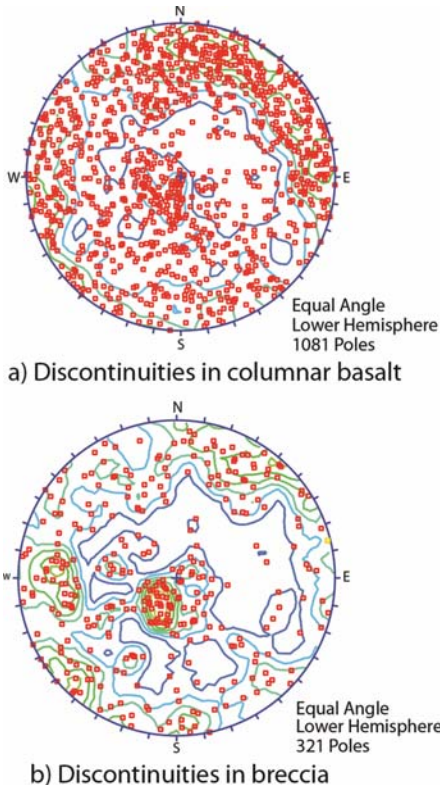

Figure 10. Cumulative stereographic projection of the poles to the discontinuity identified using terrestrial photogrammetry at all three fieldsites as a function of the geology a) columnar basalt and b) breccia, pyroclastic and tephra.

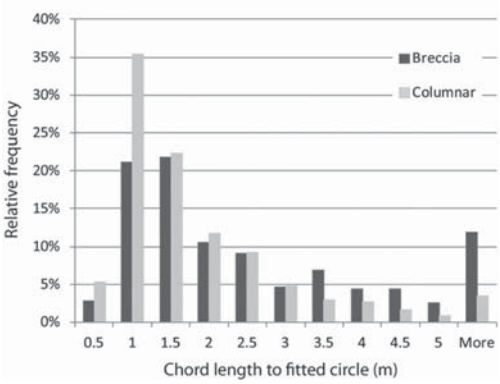

Figure 11. Relative frequency of discontinuity the trace lengths observed in the two geological units based on the terrestrial photogrammetry results.

discontinuities with shorter trace length than the thicker breccias units (Fig. 11).

5 CONCLUSIONS

The results presented in this paper demonstrate the applicability of terrestrial remote sensing techniques in acquiring discontinuity orientation information. The use of two different methods processed independently provided the opportunity to test the discontinuity sets identified. While the photogrammetry and LiDAR data sets provided similar fracturing pattern the photogrammetry was found to be better adapted to extract orientation information for shallowly dipping discontinuities. These terrestrial remote sensing techniques provided the means to rapidly and safely get structural information following major earthquake events when the potential of significant aftershocks is at its greatest.

ACKNOWLEDGEMENTS

The authors would like to thank S. Chauvin for her assistance in the field and S. Read for discussions on rock slope stability issues in the Port Hills area. Funding for this project was provided through the Landslide Hazard Platform.

REFERENCES

Allen, J., Ashford, S., Bowman, E., Bradley, B., Cox, B., Curbrinowski, M., Green, R.A., Hutchinson, T., Kavazanjian, E., Orense, R., Pender, M., Quigley, M., Wotherspoon, L. 2010. Geotechnical Reconnaissance of the 2010 Darfield (Canterbury) Earthquake. *Bulletin of the New Zealand Society for Earthquake Engineering* 43 (4): 243–320.

Barrell, D., Litchfield, N., Townsend, D., Quigley, M., Van Dissen, R., Cosgrove, R., Cox, S., Furlong, K., Villamor, P., Begg, J., Hemmings-Sykes, S., Jongens, R., Mackenzie, H., Noble, D., Stahl, T., Bilderback, E., Duffy, B., Henham, H., Klahn, A., Lang, E., Moody, L., Nicol, R., Pedley, K., Smith, A. 2011. Strike-slip ground-surface rupture (Greendale Fault) associated with the 4 September 2010 Darfield earthquake, Canterbury, New Zealand. *Quarterly Journal of Engineering Geology and Hydrogeology* 44: 283–291.

Beetham, D. 2011 Liquefaction caused by the Darfield and Christchurch earthquakes. *Geophysical Research Abstracts* EGU2011-14238.

Brideau, M.-A., Sturzenegger, M., Stead, D., Jaboyedoff, M., Lawrence, M., Roberts, N.J., Ward, B.C., Millard, T.H., Clague, J.J., 2011. Stability analysis of the 2007 Chehalis Lake landslide based on long-range terrestrial photogrammetry and airborne LiDAR data. *Landslides* DOI: 10.1007/s10346-011-0286-4.

Brown, L.J., Webber, J.H. 1992. Geology of the Christchurch urban area. Scale 1:25,000. Institute of Geology and Nuclear Sciences. Geological map GM1.

CSIRO, 2010. Sirovision version 4.1. CSIRO, Brisbane.

Davey, F. 2011. Natural hazards—the Christchurch earthquakes. *New Zealand Journal of Geology and Geophysics* 54(2): 149–150.

Fry, B., Benites, R., Reyners, M., Holden, C., Bannister, S., Kaiser, A., Williams, C., Gerstenberger, M., Ristau, J. 2011. The Christchurch Mw 6.3 earthquake: Rupture processes play a strong role in high Peak Ground Acceleration. *Geophysical Research Abstracts*, EGU2011-14231.

Gledhill, K., Ristau, J., Reyners, M., Fry, B., Holden, C. 2011. The Darfield (Canterbury, New Zealand) Mw 7.1 Earthquake of September 2010: A preliminary seismological report. *Seismological Research Letters* 52(3): 378–386.

Hancox, G., Perrin, N. 2011. Report of landslide reconnaissance flight of 24 February 2011 following the Mw 6.3 Christchurch Earthquake of 22 February 2011. GNS Science Immediate Report, Job Number 460 W6303. Available on www.geonet.org.nz.

Hancox, G., Massey, C., Perrin, N. 2011. Landslides and related ground damage caused by the Mw 6.3 Christchurch Earthquake of 22 February 2011. *New Zealand Geomechanics News Issue* 81: 53–67.

Haneberg, W.C., 2008. Using close range terrestrial digital photogrammetry for 3-D rock slope modeling and discontinuity mapping in the United States. *Bulletin of Engineering Geology and the Environment* 67: 457–469.

Jaboyedoff, M., Baillifard, F., Couture, R., Locat J., Locat, P., 2004. Toward preliminary hazard assessment using DEM topographic analysis and simple mechanic modeling. In Lacerda et al. (eds.), *Landslides Evaluation and Stabilization*, 191–197.

Jaboyedoff, M., Oppikofer, T., Abellan, A., Derron, M.-H., Loye, A., Metzger, R., Pedrazzini, A., 2011. Use of LiDAR in landslide investigations: a review. *Natural Hazards*. DOI: 10.10007/s11069-010-9634-2.

Jaboyedoff, M., Couture, R., Locat, J. 2009. Structural analysis of Turtle Mountain (Alberta) using digital elevation model: Toward a progressive failure. *Geomorphology* 103, 5–16.

Maconochie, A.P., Soole, P., Simmons, J. 2010. Validation of a simple one person method for structural mapping using Sirovision, Bowen Basin Symposium 2010, Mackay, Australia, 181–184.

Massey, C.I., Dellow, G.D. 2011. Rockfalls and landslides triggered by the February 2011 Christchurch (NZ) earthquake: the GeoNet response. *Geophysical Research Abstracts* EGU2011-14236.

Massey, C.I., Petley, D., Rosser, N. 2010. Harper Hills Landslides, Canterbury. GeoNet Landslide Response, 8p. available online at: www.geonet.org.nz.

Oppikofer, T., Jaboyedoff, M., Blikra, L.H., Derron, M.-H., Metzger, R. 2009. Characterization and monitoring of the Aknes rockslide using terrestrial laser scanning. *Natural Hazards and Earth System Sciences* 9: 1003–1019.

Oppikofer, T., Jaboyedoff, M., Pedrazzini, A., Derron, M.-H., Blikra, L.H. 2011. Detailed DEM analysis of a rockslide scar to characterize the basal sliding surface of active rockslides. *Journal of Geophysical Research*, F02016.

Pedrazzini, A., Oppikofer, T., Jaboyedoff, M., Guell i Pons, M. 2010. Assessment of rockslide and rockfall problems in an active quarry: Case study of the Arvel quarry (Western Switzerland). In Zhao et al. (eds.), EUROCK 2010, Lausanne, Switzerland, 593–596.

Reyners, M. 2011. Lessons from the destructive Mw6.3 Christchurch, New Zealand, earthquake. *Seismological Research Letters* 82(3): 371–372.

Sewell, R.J., Weaver, S.D., Reay, M.B. 1992. Geology of the Banks Peninsula. Scale 1:100 000. Institute of Geology and Nuclear Sciences, Geological map GM3.

Sturzenegger, M., Stead, D. 2009a. Close-range terrestrial digital photogrammetry and terrestrial laser scanning for discontinuity characterization on rock cuts. *Engineering Geology* 106: 163–182.

Sturzenegger, M., Stead, D. 2009b. Quantifying discontinuity orientation and persistence on high mountain rock slopes and large landslides using terrestrial remote sensing techniques. *Natural Hazards and Earth System Sci* 9: 267–287.